Rare and new compounds in the Ni-Cu-Sb-As system: first occurrence in the Gomati ophiolite, Greece

Micol Bussolesi [1,*], Federica Zaccarini [2], Giovanni Grieco [1], Evangelos Tzamos [3]

[1] Department of Earth Sciences, University of Milan, via S. Botticelli 23, 20133, Milan, Italy
[2] Department of Applied Geological Sciences and Geophysics, University of Leoben, A-8700 Leoben, Austria
[3] Department of Geology and Geoenvironment, National and Kapodistrian University of Athens, Zografou Campus, 15784, Athens, Greece

ABSTRACT

The Gomati ophiolite (Northern Greece) is located in the Serbo-Macedonian Massif, in the Hellenides orogenic belt. It consists of altered peridotites hosting scattered chromitite bodies. The ultramafics are enclosed in Silurian gneisses and schists, and are partially in contact with late Cenozoic granites. The present work focuses on accessory minerals in the Ni-Cu-Sb-As system, found in a chloritized clinopyroxenite in contact with chromitite. The electron microprobe analyses revealed the presence of known minerals such as orcelite ($Ni_{5-x}As_2$) and breithauptite (NiSb) and new phases that cluster around the following compositions: Ni_3As, $Ni_5(As,Sb)_2$, $(Ni,Cu)_{5-x}(Sb,As)_2$, $(Ni,Cu)_2(Sb,As)$, and $(Ni,Cu)_{11}(Sb,As)_8$. The compound $(Ni,Cu)_{5-x}(Sb,As)_2$ may correspond to a Cu-rich Sb dominant variant of this phase. A phase corresponding to $(Ni,Cu)_2(Sb,As)$ was first described in the Tulameen complex of Canada. A phase with stoichiometry Ni_3As was formerly known as the mineral dienerite, later discredited by the IMA and only recently under revalidation. The compound $(Ni,Cu)_{11}(Sb,As)_8$ probably represents a Cu-rich Sb-dominant analogue of the mineral maucherite ($Ni_{11}As_8$). The mineral assemblage in the Gomati ophiolite is puzzling. While ultramafic rocks contain Ni and As of magmatic origin, the presence of Sb, Ag, Au and Cu minerals could be indicative of a metasomatic enrichment, probably linked to the presence of fluids emanating from the granite body or a nearby porphyry copper mineralization.

Keywords: new compounds; Ni-Cu-Sb-As system; chromitite; ophiolite; Gomati; Greece.

INTRODUCTION

According to the list officially released on March 2019 by the Commission of New Minerals Nomenclature and Classification (CNMNC) of the International Mineralogical Association (IMA) (http://cnmnc.main.jp/) only eighteen minerals, described in the system Ni-Cu-Sb-As, have been accepted as valid species (Table 1). In particular, five of them are Cu-arsenides, i.e. algodonite Cu_6As (Bayliss, 1990 and references therein), domeykite Cu_3As (Iglesias and Nowacki, 1977), koutekite Cu_5As_2 (Johan, 1958; Liebisch and Schubert, 1971), novakite $(Cu,Ag)_{21}As_{10}$ (Johan and Hak, 1961) and paxite Cu_2As_3 (Johan, 1961), and seven are Ni-arsenides namely krutovite $NiAs_2$ (Vinogradova et al., 1976), maucherite $Ni_{11}As_8$ (Makovicky and Merlino, 2009), nickeline NiAs (Thompson et al., 1988) nickelskutterudite $(Ni,Co,Fe)As_3$

Table 1. IMA approved minerals in the Ni-Cu-Sb-As system.

Mineral	Ideal formula	Crystal system	References
Cu-dominant			
Algodonite	Cu_6As	Hexagonal	Bayliss, 1990 and references therein
Domeykite	Cu_3As	Isometric	Iglesias and Nowacki, 1977
Koutekite	Cu_5As_2	Hexagonal	Johan, 1958; Liebisch and Schubert, 1971
Novakite	$(Cu,Ag)_{21}As_{10}$	Monoclinic	Johan and Hak, 1961
Paxite	Cu_2As_3	Monoclinic	Johan, 1961
Cuprostibite	$Cu_2(Sb,Tl)$	Tetragonal	Pearson, 1985
Ni-dominant			
Krutovite	$NiAs_2$	Isometric	Vinogradova et al., 1976
Maucherite	$Ni_{11}As_8$	Tetragonal	Makovicky and Merlino, 2009
Nickeline	$NiAs$	Hexagonal	Thompson et al., 1988
Nickelskutterudite	$(Ni,Co,Fe)As_3$	Isometric	Schumer et al., 2017
Orcelite	$Ni_{5-x}As_2$	Hexagonal	Bindi et al. 2014 and references therein
Pararammelsbergite	$NiAs_2$	Orthorhombic	Peacock, 1939; Peacock and Dadson, 1940
Rammelsbergite	$NiAs_2$	Orthorhombic	Peacock, 1939; Peacock and Dadson, 1940
Breithauptite	$NiSb$	Hexagonal	Palache et al., 1944
Nisbite	$NiSb_2$	Orthorhombic	Cabri et al., 1970
Others			
Zlatogorite	$CuNiSb_2$	Trigonal	Kabalov et al., 1994
Stibarsen	$SbAs$	Trigonal	Bayliss, 1991 and reference therein
Paradocrasite	$Sb_2(Sb,As)_2$	Monoclinic	Leonard and Finney, 1971

(Schumer et al., 2017), orcelite $Ni_{5-x}As_2$, (Bindi et al., 2014 and references therein) pararammelsbergite $NiAs_2$ and rammelsbergite $NiAs_2$ (Peacock, 1939; Peacock and Dadson, 1940). Copper and nickel antimonides are less abundant and only four of them have been accepted so far: zlatogorite $CuNiSb_2$ (Kabalov et al., 1994) cuprostibite $Cu_2(Sb,Tl)$ (Pearson, 1985), breithauptite $NiSb$ (Palache et al., 1944) and nisbite $NiSb_2$ (Cabri et al., 1970). Two minerals, stibarsen $SbAs$ (Bayliss, 1991 and references therein) and paradocrasite $Sb_2(Sb,As)_2$ (Leonard et al., 1971) contain only antimony and arsenic. Nixon et al. (1990) reported the presence of breithauptite and two new minerals characterized by the ideal formulae $(Ni,Cu)_2Sb$ and Ni_3Sb in chromitite from the Alaskan-type Tulameen complex of Canada. More recently, Tredoux et al. (2016), described several minerals in the Ni-Sb-As system from the Bon Accord oxide body, South Africa. Electron microprobe analyses indicated that, although some of these are known minerals, such as breithauptite and orcelite, most of them exhibit a stoichiometry close to: Ni_3Sb, $Ni_3(Sb,As)$, Ni_3As, $Ni_5(Sb,As)_2$, $Ni_7(Sb,As)_3$ and $Ni_{11}(Sb,As)_8$. The phases reported by Tredoux et al. (2016) are known in the synthetic systems, but not in nature. All

the grains described by Nixon et al. (1990) and Tredoux et al. (2016) very likely represent new mineral species, but they are too small to be investigated by X-ray diffraction. However, these Authors demonstrated that the minerals in the system Ni-Sb-As are much more compositionally complex than previously reported.

In this contribution we report the occurrence of rare accessory minerals, including phases that contain Ni-Cu-Sb-As as major elements, found in podiform chromitites from the Gomati ophiolite, Greece. Their composition and those of associated minerals, as well as mineralogical assemblage and genetic implications are discussed.

SAMPLE PROVENANCE

The accessory minerals described in the present work were observed in a sample that represents the contact between massive chromitite and the associated silicate rock collected in the Gomati ophiolite (Figure 1).

The Gomati ophiolite is an ultramafic body cropping out in the Chalkidiki peninsula, Northern Greece (Figure 1). The body is comprised in the Serbo-Macedonian-Massif (SMM), one of the geotectonic terranes composing the Hellenides orogeny. The Serbo-Macedonian Massif
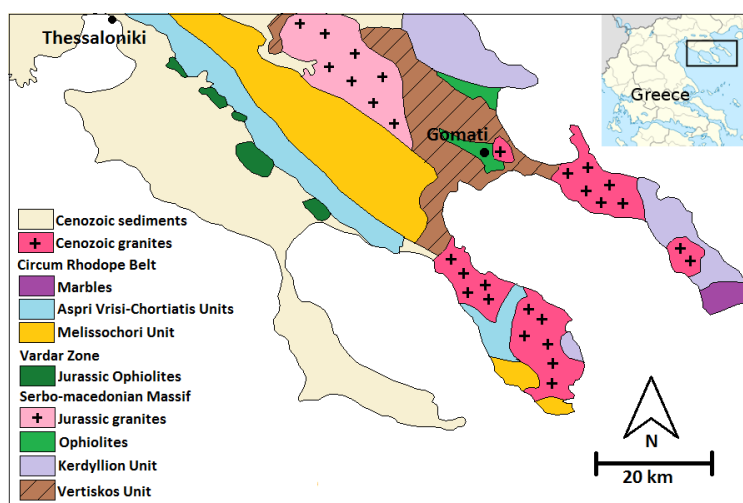
Figure 1. Simplified geological map of the Chalkidiki peninsula (modified after Melfos and Voudouris, 2012).

consists of amphibolite-facies metamorphic rocks of continental and oceanic origin, forming the basement of the Alpine orogenic belt, and recording a late Mesozoic deformation episode followed by Cenozoic extension (Bonev et al., 2012, 2018; Ricou et al., 1998). The mafic-ultramafic rocks of the SMM have an unclear origin, interpreted either as a Triassic rift (Dixon and Dimitriadis, 1984) or as the remnant of the Permian Palaeothetys suture (Şengör et al., 1984). The SMM is divided into a lower unit (Kerdyllion) and an upper unit (Vertiskos), and it is characterized by the presence of Cenozoic granitic intrusions. The Kerdyllion unit, cropping out in the eastern part, is composed of gneisses intruded by granitoid rocks. The Vertiskos unit, cropping out in the central part of the SMM, consists of an alternation of gneisses and schists hosting mafic-ultramafic bodies (Dixon and Dimitriadis, 1984; Kockel, 1977). Several ophiolite outcrops have been found into the Vertiskos unit, close to the Gomati village, in Paivouni, Tripes, Papaloni, Moutsares and Kranies (Christodoulou, 1980; Economou, 1984).

The Gomati ophiolite consists of serpentinized peridotites with scattered chromitite occurrences presenting massive, schlieren and disseminated textures. Chromitites and related rocks are heavily altered and show intense chloritization and the development of ferrian-chromite. Preserved primary silicates consist mainly of forsteritic olivine and diopsidic clinopyroxene.

METHODOLOGY

Chromite, silicates and accessory minerals were analyzed by electron microprobe using a Superprobe Jeol JXA 8200 at the Eugen F. Stumpfl Laboratory at the University of Leoben, Austria, using both ED and WD systems. Back-scattered electron images and X-ray elemental distribution maps were obtained using the same instrument and the same conditions. During the analyses of chromite and silicates, the electron microprobe was operated in the WDS mode, with an accelerating voltage of 15 kV of and beam current of 10 nA. The elements (Na, Mg, K, Al, Si, Ca, Ti, V, Cr, Zn, Mn, Fe, and Ni) were analyzed using the Kα line. Specimens of chromite, rhodonite, ilmenite, albite, pentlandite, wollastonite, kaersutite, sphalerite, and metallic vanadium were used as standards. The following diffracting crystals were used: TAP for Na, Mg, and Al; PETJ for K, Si, and Ca; and LIFH for Ti, V, Cr, Zn, Mn, Fe, and Ni. The peak and backgrounds counting times were 20 and 10 s, respectively, for the major elements. Selected analyses of chromite and silicates (clinopyroxene and chlorite) are listed in Tables 2, 3 and 4.

The accessory minerals were carefully investigated with a reflected-light microscope at 250-800X magnification, at the University of Leoben, Austria. The grains larger than 10 microns were quantitatively analyzed in the WDS mode. Analytical conditions were 20 kV accelerating voltage, 10 nA beam current, and beam diameter of about 1 micron. The peak and background counting times were 20 and 10s, respectively. The following lines were selected: Kα for S, Ni, Fe and Cu, Mα for Pb and Lα for As and Sb. The standards employed were: galena (Pb), chalcopyrite (Cu), pyrite (Fe,S), stibnite (Sb), synthetic GaAs (As), and millerite (Ni). The composition of accessory minerals are presented in Tables 5, 6 and 7.

RESULTS
Composition and texture of chromite and silicate minerals

The studied samples consist of massive chromitite, with up to 30% by volume interstitial silicates, and disseminated
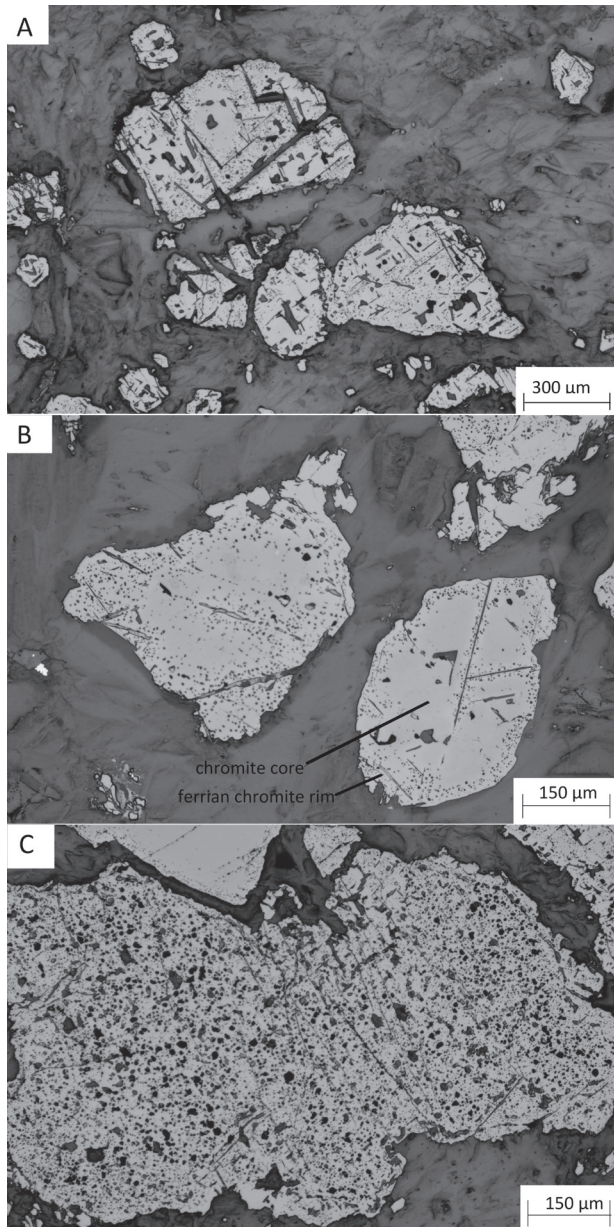
Figure 2. Reflected-light microscopy digital images showing the texture and alteration rate of Gomati chromitites; bright grey = chromite, dark gray = chlorite and minor serpentine and talc.

chromitite. The silicate matrix is composed mainly of secondary chlorite accompanied by minor clinopyroxene relicts, serpentine and talc. Both, the massive and disseminated chromitites show a peculiar texture (Figure 2 A,B,C) characterized by polygonal and rounded grains that contain abundant inclusions of chlorite generally oriented along the crystal planes of the host chromite (Figure 2 A,B). Inclusions of magmatic silicates, such as olivine, pyroxene and amphibole are missing. The original texture of the Gomati chromitite has been modified by

significant alteration of the chromite crystals. They show a complex zoning, consisting of unaltered chromite cores within partially altered grains, replaced by ferrian-chromite along rims and cracks (Figure 2 B,C). Several grains of chromite have been totally altered and the original magmatic composition has been completely modified. With proceeding alteration, the rim of ferrian-chromite becomes porous and intimately intergrown with secondary silicates (Figure 2 B,C). In some chromite crystals, the pores filled with chlorite, serpentine and talc are widespread in all the surface of the crystals (Figure 2C).

Selected analyses of fresh and altered chromite crystals are listed in Table 2 and plotted in the binary diagram of Figure 3A. According to this diagram, all the analyzed spinels plot in the field of chromite, with altered grains slightly enriched in chromium. Spinel mineral chemistry is rather heterogeneous from core to rim, due to strong alteration in ferrian-chromite (Table 2). Spinel cores show homogeneous compositions, with Cr_2O_3 and Al_2O_3 contents of 51.13-53.15 wt% and 10.04-12.26 wt%, respectively. MgO content is comprised between 5.05 and 5.78 wt%, and FeO content is between 25.03 and 25.99 wt%. Calculated Fe_2O_3 contents range from 3.76 to 5.10 wt%. Ferrian-chromite rims present Cr_2O_3 and Al_2O_3 contents of 52.98-61.66 wt% and 1.69-8.96 wt%, respectively. MgO content is comprised between 3.25 and 4.86 wt%, and FeO content ranges between 26.31 and 27.93 wt%. Calculated Fe_2O_3 content ranges between 4.80 and 6.71 wt%.

The silicates in which the disseminated chromite is embedded consist mainly of chlorite and clinopyroxene with subordinate serpentine and talc. The interstitial silicates in the massive chromite samples are completely altered (Figure 2). The analyses of clinopyroxene are reported in the ternary diagram of Figure 3B and in Table 3. Their composition plots almost entirely in the diopside field, with a few exceptions of augite (Figure 3B). Clinopyroxene mineral chemistry is characterized by CaO content between 20.71 and 25.95 wt%, MgO content of 17.50-23.30 wt% and FeO content between 0.53 and 0.90 wt%.

Chlorite substituting primary silicates has FeO contents between 1.80 and 2.67 wt% (Table 4). The composition falls in the field of clinochlore (Figure 3C). However, due the presence of abundant Cr_2O_3 (1.66-4.73 wt%), the term chromian clinochlore to define the analyzed chlorite in the Gomati samples is more appropriate. It is well known that the compositional variations of chlorite can reflect physicochemical conditions in which the mineral crystallized (Cathelineau and Nieva, 1985; Cathelineau, 1988; Kranidiotis and MacLean, 1987; Zang and Fyfe, 1995). It has been established that the amount of ^{IV}Al substituting Si in the tetrahedral site is controlled by temperature. Therefore, the geothermometric equation
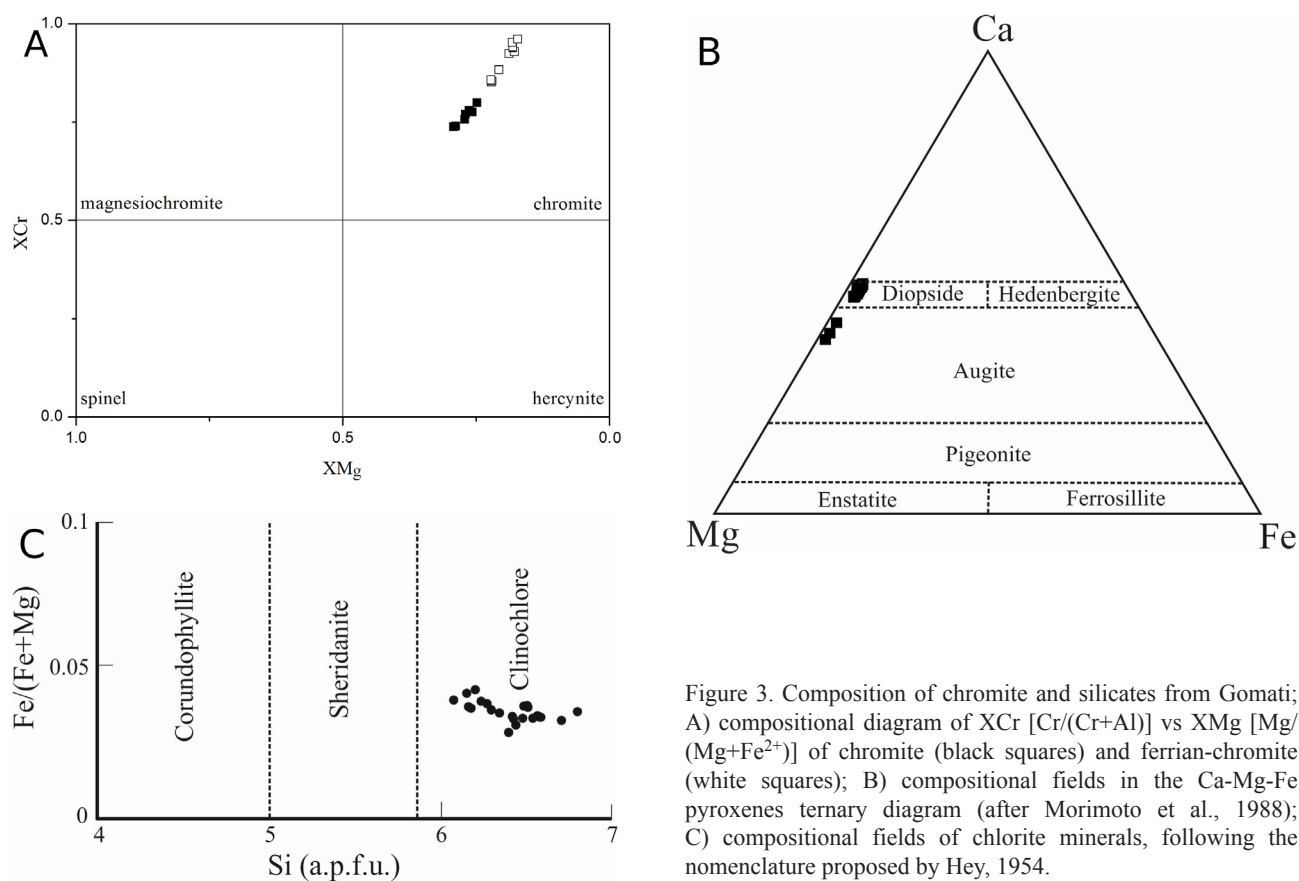
Figure 3. Composition of chromite and silicates from Gomati; A) compositional diagram of XCr [Cr/(Cr+Al)] vs XMg [Mg/(Mg+Fe^{2+})] of chromite (black squares) and ferrian-chromite (white squares); B) compositional fields in the Ca-Mg-Fe pyroxenes ternary diagram (after Morimoto et al., 1988); C) compositional fields of chlorite minerals, following the nomenclature proposed by Hey, 1954.

Table 2. selected microprobe analyses (wt%) of chromite; chr: magmatic chromite; Fe-chr: altered chromite.

	TiO_2	Al_2O_3	Cr_2O_3	V_2O_3	Fe_2O_3	FeO	MnO	MgO	NiO	ZnO	Tot	Mg#	Cr#	Fe^{3+}#
1-chr	0.36	11.22	52.10	0.17	5.10	25.55	0.41	5.33	0.08	0.01	100.34	0.27	0.76	0.07
2-chr	0.44	12.23	51.43	0.18	4.06	25.04	0.32	5.78	0.07	bdl	99.54	0.29	0.74	0.05
3-chr	0.39	12.20	51.13	0.18	4.16	25.03	0.24	5.77	0.04	bdl	99.14	0.29	0.74	0.05
4-chr	0.43	10.31	53.15	0.21	4.98	25.99	0.36	5.05	0.06	0.10	100.61	0.26	0.78	0.06
5-chr	0.33	12.25	51.99	0.17	3.76	25.03	0.29	5.69	0.04	0.11	99.67	0.29	0.74	0.05
6-Fe-chr	0.45	3.25	59.14	0.18	6.51	27.36	0.37	3.55	bdl	bdl	100.80	0.19	0.92	0.09
7-Fe-chr	0.34	3.15	61.40	0.14	5.02	27.93	0.40	3.40	bdl	bdl	101.78	0.18	0.93	0.07
8-Fe-chr	0.36	1.69	61.66	0.17	6.57	27.81	0.37	3.25	0.03	0.05	101.94	0.17	0.96	0.09
9-Fe-chr	0.35	1.99	60.76	0.15	6.38	27.16	0.43	3.39	0.07	bdl	100.67	0.18	0.95	0.09
10-Fe-chr	0.40	2.55	60.21	0.18	5.95	27.33	0.36	3.40	0.05	0.14	100.56	0.18	0.94	0.08

Fe_2O_3 and FeO calculated assuming perfect stoichiometry.

based on this substitution proposed by Cathelineau and Nieva (1985) has been applied to evaluate the crystallization temperature of the chlorite found in the Gomati chromitite. Calculated temperatures give values comprised between 220-310 °C, with an average of 273 °C, and their thermometric significance was not affected by alkalis contamination (Frimmel, 1997), being the values of Ca+Na+K (at%) less than 0.1 (Table 4).

PM

Table 3. selected microprobe analyses (wt%) of clinopyroxene.

	SiO$_2$	TiO$_2$	Al$_2$O$_3$	FeO	MnO	MgO	CaO	Cr$_2$O$_3$	Total	Wo	En	Fs
CPX-1	55.49	0.07	0.01	0.65	0.02	18.00	25.78	0.05	100.08	0.50	0.49	0.01
CPX-2	54.59	0.01	0.13	0.79	0.04	18.46	25.20	0.05	99.27	0.49	0.50	0.00
CPX-3	54.50	0.01	0.03	0.75	bdl	18.44	25.96	0.02	99.76	0.50	0.50	0.00
CPX-4	54.62	0.05	0.04	0.70	0.01	18.29	25.45	0.04	99.24	0.50	0.50	0.00
CPX-5	55.22	0.08	0.06	0.72	0.01	19.00	24.48	0.04	99.68	0.47	0.51	0.01
CPX-7	54.01	bdl	0.08	0.68	bdl	18.61	24.55	0.06	98.01	0.48	0.51	0.00
CPX-23	54.44	0.03	0.09	0.53	0.02	18.27	24.83	0.02	98.31	0.49	0.50	0.01
CPX-25	54.75	0.11	0.06	0.63	bdl	18.47	24.89	0.10	99.09	0.49	0.50	0.01
CPX-40	53.79	bdl	0.01	0.70	0.02	18.14	25.23	0.32	98.21	0.50	0.50	0.00
CPX-44	53.87	0.01	0.04	0.73	0.01	18.06	25.42	0.05	98.19	0.50	0.50	0.00

Table 4. selected microprobe analyses (wt%) of chlorite.

	SiO$_2$	TiO$_2$	Al$_2$O$_3$	FeO	MnO	MgO	CaO	Na$_2$O	K$_2$O	Cr$_2$O$_3$	Total
CHL-60	35.39	0.02	8.24	1.95	0.01	33.43	0.10	bdl	bdl	2.02	81.15
CHL-35	31.75	0.02	10.74	2.04	bdl	32.70	0.03	0.03	bdl	4.33	81.63
CHL-62	33.09	0.01	11.05	2.10	0.01	33.23	0.05	0.01	bdl	2.89	82.44
CHL-34	30.66	0.01	11.97	2.33	0.02	33.20	0.02	0.01	bdl	4.35	82.56
CHL-39	30.94	0.01	12.30	2.30	bdl	33.21	0.02	bdl	bdl	4.17	82.98
CHL-53	34.10	0.01	10.47	2.12	bdl	34.69	0.01	bdl	bdl	1.66	83.09
CHL-29	31.07	0.04	12.31	2.67	0.02	32.81	0.06	bdl	bdl	4.15	83.12
CHL-33	30.67	0.01	12.60	2.52	0.02	33.92	0.02	0.01	bdl	4.04	83.81
CHL-37	31.88	0.01	11.49	2.29	bdl	33.70	0.00	bdl	bdl	4.53	83.91
CHL-32	32.20	0.02	11.43	2.23	bdl	33.73	0.00	bdl	bdl	4.35	83.97

Table 4. ...Continued

	Si	Ti	Al(IV)	Al(VI)	Fe	Mn	Mg	Ca	Na	K	Cr	T(°C)
CHL-60	7.11	0.00	0.89	1.06	0.33	0.00	10.01	0.02	0.00	0.00	0.32	218
CHL-35	6.43	0.00	1.57	1.00	0.35	0.00	9.88	0.01	0.01	0.00	0.69	263
CHL-62	6.59	0.00	1.41	1.19	0.35	0.00	9.87	0.01	0.00	0.00	0.45	250
CHL-34	6.17	0.00	1.83	1.01	0.39	0.00	9.96	0.00	0.00	0.00	0.69	294
CHL-39	6.19	0.00	1.81	1.08	0.38	0.00	9.90	0.00	0.00	0.00	0.66	288
CHL-53	6.71	0.00	1.29	1.14	0.35	0.00	10.18	0.00	0.00	0.00	0.26	266
CHL-29	6.21	0.01	1.79	1.11	0.45	0.00	9.77	0.01	0.00	0.00	0.66	280
CHL-33	6.08	0.00	1.92	1.03	0.42	0.00	10.03	0.00	0.00	0.00	0.63	309
CHL-37	6.30	0.00	1.70	0.98	0.38	0.00	9.93	0.00	0.00	0.00	0.71	282
CHL-32	6.35	0.00	1.65	1.01	0.37	0.00	9.92	0.00	0.00	0.00	0.68	276

Composition and mineralogical assemblages of the minerals in the Ni-Cu-Sb-As system and other accessory phases

Based on their chemical composition, the following species were recognized at Gomati: heazlewoodite (Table 5), chalcocite, shandite, galena, orcelite, breithauptite, and a Cu-Au alloy, probably tetraauricupride. Several unnamed and potentially new minerals in the Ni-Cu-Sb-As system have been also found, and they cluster around the following compositions: Ni_3As, $Ni_5(As,Sb)_2$, $(Ni,Cu)_{5-x}(Sb,As)_2$, $(Ni,Cu)_2(Sb,As)$, $(Ni,Cu)_{11}(Sb,As)_8$ (Figure 4 and Tables 6 and 7).

The composition of the analysed grains has been plotted, as atomic proportions, in the ternary diagram of Figure 4 and compared with the grains found in the Bon

Table 5. Selected electron microprobe analyses of heazlewoodite.

| Wt%	S	Ni	Fe	Cu	Total
GOM2B-SULF-19	28.12	72.35	0.23	0.06	100.75
GOM2BSULF65	26.51	72.59	0.09	0.04	99.23
GOM2BSULF59	27.00	73.48	0.10	0.05	100.67
GOM2B-SULF-2	26.32	74.17	0.14	0.09	100.77
GOM2BSULF67	26.52	73.07	0.09	0.06	99.73
GOM2B-SULF-11	25.78	73.24	0.34	bdl	99.36
GOM2BSULF61	26.27	73.59	0.07	0.06	99.99
GOM2B-SULF-39	26.12	73.60	0.18	0.06	99.96
GOM2B-SULF-28	26.00	73.70	0.12	0.12	99.94
GOM2BSULF64	26.28	73.95	0.17	0.06	100.47
GOM2B-SULF-43	25.72	73.98	0.14	0.10	99.94
GOM2B-SULF-24	25.86	74.41	0.13	0.04	100.46
GOM2B-SULF-17	25.79	74.55	0.14	0.05	100.53
GOM2B-SULF-25	25.49	74.99	0.12	0.01	100.61
GOM2B-SULF-12	25.91	75.11	0.19	bdl	101.22
GOM2B-SULF-36	25.83	75.12	0.19	0.07	101.21
GOM2B-SULF-33	25.78	75.49	0.17	bdl	101.44
apfu	**S**	**Ni**	**Fe**	**Cu**	**Total**
GOM2B-SULF-19	2.07	2.91	0.01	0.00	5.00
GOM2BSULF65	2.00	2.99	0.00	0.00	5.00
GOM2BSULF59	2.01	2.99	0.00	0.00	5.00
GOM2B-SULF-2	1.96	3.02	0.01	0.00	5.00
GOM2BSULF67	1.99	3.00	0.00	0.00	5.00
GOM2B-SULF-11	1.95	3.03	0.01	0.00	5.00
GOM2BSULF61	1.97	3.02	0.00	0.00	5.00
GOM2B-SULF-39	1.96	3.03	0.01	0.00	5.00
GOM2B-SULF-28	1.96	3.03	0.00	0.00	5.00
GOM2BSULF64	1.97	3.02	0.01	0.00	5.00
GOM2B-SULF-43	1.94	3.05	0.01	0.00	5.00
GOM2B-SULF-24	1.94	3.05	0.01	0.00	5.00
GOM2B-SULF-17	1.94	3.06	0.01	0.00	5.00
GOM2B-SULF-25	1.92	3.08	0.01	0.00	5.00
GOM2B-SULF-12	1.93	3.06	0.01	0.00	5.00
GOM2B-SULF-36	1.93	3.06	0.01	0.00	5.00
GOM2B-SULF-33	1.92	3.07	0.01	0.00	5.00
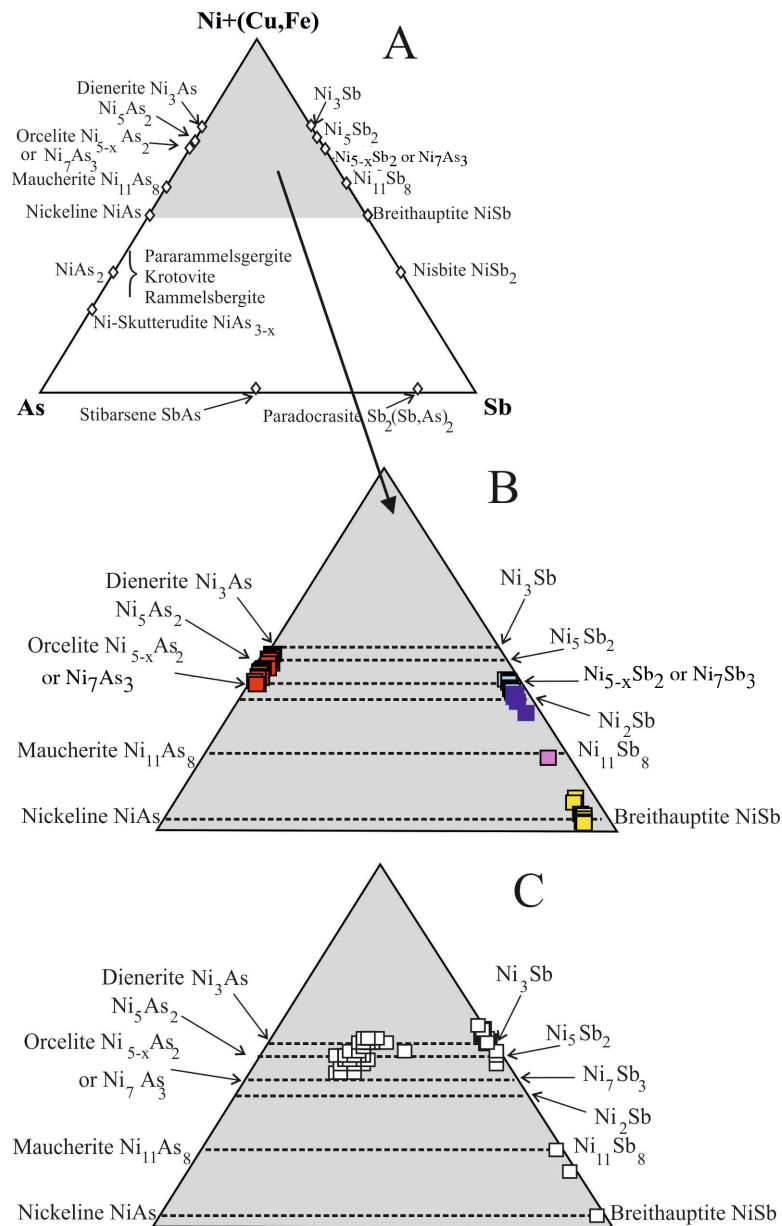
Figure 4. Compositional fields of arsenides and antimonides in the (Ni+Cu+Fe)-Sb-As system; A) Plot of the ideal composition of the minerals accepted by CNMNC and those proposed by Tredoux et al. (2016); B) Composition of the Gomati minerals (present work); C) Composition of the Bon Accord minerals (Tredoux et al., 2016).

Accord complex of South Africa by Tredoux et al. (2014). This diagram shows that several grains of Gomati are very similar in composition to those of Bon Accord. However, the Sb-As substitution described in the Bon Accord minerals is not present in the analysed grains. According to the compositions listed in Tables 6 and 7, Fe content in the Gomati new minerals is invariably low (less than 0.6 wt%), whereas the new minerals with dominant Sb are enriched in Cu, up to 13.59 wt%.

The accessory minerals are commonly less than 15 μm

in size and most of them are located at the contact between chromian clinochlore and clinopyroxene and, more rarely, as inclusions in ferrian-chromite (Figures 5 A-E and 6 A-C). Chalcocite, shandite and galena occur only as single grains (Figure 5 A,B), whereas tetraauricupride has been found in a heterogeneous grain composed of heazlewoodite and a Ni-Cu-Fe antimonide (Figure 5C) The other accessory minerals occur either as single or composite grains (Figures 5 A-E and 6 A-C).

As most of the studied grains are very small, the optical

Table 6. Selected electron microprobe analyses of Ni-arsenides.

Wt%	As	S	Ni	Fe	Cu	Sb	Total
Ni$_3$(As,Sb)							
GOM2B-SULF-9	31.47	bdl	66.54	0.04	0.15	0.87	99.07
GOM2B-SULF-10	31.91	0.02	67.70	0.09	0.17	0.88	100.76
GOM2B-SULF-13	31.52	bdl	67.41	0.13	0.10	0.78	99.93
GOM2B-SULF-18	31.67	0.02	65.33	0.23	0.25	1.55	99.06
GOM2B-SULF-32	32.09	bdl	69.28	0.14	0.11	1.18	102.80
GOM2B-SULF-42	32.10	bdl	68.07	0.13	0.13	0.80	101.23
GOM2B-SULF-60	31.71	bdl	68.59	0.16	0.17	0.91	101.55
GOM2B-SULF-66	32.05	0.02	65.99	0.06	0.14	1.20	99.47
GOM2B-SULF-68	32.19	bdl	66.38	0.14	0.60	0.75	100.05
GOM2B-SULF-71	32.00	bdl	65.43	0.17	0.28	1.90	99.78
Ni$_5$(As,Sb)$_2$							
GOM2B-SULF-27	32.90	0.01	66.38	0.10	0.22	1.17	100.79
GOM2B-SULF-52	34.19	0.01	65.15	0.11	0.20	0.71	100.36
GOM2B-SULF-53	33.86	0.03	65.64	0.12	0.12	0.69	100.47
GOM2B-SULF-69	32.85	0.03	64.77	0.17	0.14	1.80	99.78
Ni$_{5-x}$(As,Sb)$_2$ (orcelite)							
GOM2B-SULF-38	35.71	0.03	64.91	0.20	0.04	0.75	101.63
GOM2B-SULF-41	35.21	bdl	64.55	0.25	0.15	0.65	100.82
GOM2B-SULF-45	34.70	0.01	64.71	0.23	0.14	0.71	100.49
GOM2B-SULF-47	35.33	0.04	62.52	0.20	0.06	1.64	99.80
GOM2B-SULF-49	34.60	0.03	65.04	0.15	0.19	0.71	100.71
GOM2B-SULF-54	34.35	0.01	62.89	0.13	0.33	1.77	99.47
GOM2B-SULF-58	35.80	0.02	63.37	0.26	0.06	0.82	100.34
apfu	As	S	Ni	Fe	Cu	Sb	Total
Ni$_3$(As,Sb)							
GOM2B-SULF-9	1.07	0.00	2.90	0.00	0.01	0.02	4.00
GOM2B-SULF-10	1.07	0.00	2.90	0.00	0.01	0.02	4.00
GOM2B-SULF-13	1.07	0.00	2.91	0.01	0.00	0.02	4.00
GOM2B-SULF-18	1.09	0.00	2.86	0.01	0.01	0.03	4.00
GOM2B-SULF-32	1.06	0.00	2.91	0.01	0.00	0.02	4.00
GOM2B-SULF-42	1.07	0.00	2.90	0.01	0.01	0.02	4.00
GOM2B-SULF-60	1.05	0.00	2.91	0.01	0.01	0.02	4.00
GOM2B-SULF-66	1.09	0.00	2.87	0.00	0.01	0.03	4.00
GOM2B-SULF-68	1.09	0.00	2.87	0.01	0.02	0.02	4.00
GOM2B-SULF-71	1.09	0.00	2.85	0.01	0.01	0.04	4.00
Ni$_5$(As,Sb)$_2$							
GOM2B-SULF-27	1.94	0.00	4.99	0.01	0.02	0.04	7.00
GOM2B-SULF-52	2.02	0.00	4.93	0.01	0.01	0.03	7.00
GOM2B-SULF-53	2.00	0.00	4.95	0.01	0.01	0.02	7.00
GOM2B-SULF-69	1.96	0.00	4.94	0.01	0.01	0.07	7.00
Ni$_{5-x}$(As,Sb)$_2$ with x=0.23 (orcelite)							
GOM2B-SULF-38	2.02	0.00	4.70	0.01	0.00	0.03	6.77
GOM2B-SULF-41	2.01	0.00	4.71	0.02	0.01	0.02	6.77
GOM2B-SULF-45	1.99	0.00	4.73	0.02	0.01	0.02	6.77
GOM2B-SULF-47	2.05	0.01	4.63	0.02	0.00	0.06	6.77
GOM2B-SULF-49	1.98	0.00	4.74	0.01	0.01	0.02	6.77
GOM2B-SULF-54	2.00	0.00	4.67	0.01	0.02	0.06	6.77
GOM2B-SULF-58	2.06	0.00	4.65	0.02	0.00	0.03	6.77

Table 7. Selected electron microprobe analyses of Ni-Cu antimonides.

| Wt%	As	S	Ni	Fe	Cu	Sb	Total
$(Ni,Cu)_{5-x}(Sb,As)_2$							
GOM2B-SULF-1	1.19	bdl	41.07	0.08	12.44	46.23	101.02
GOM2B-SULF-16	0.98	0.03	40.91	0.08	12.55	47.15	101.70
GOM2B-SULF-21	1.06	bdl	39.87	0.13	12.60	46.44	100.10
$(Ni,Cu)_2(Sb,As)$							
GOM2B-SULF-20	1.21	bdl	38.97	0.13	12.76	47.59	100.67
GOM2B-SULF-22	1.15	bdl	39.51	0.11	12.92	47.92	101.62
GOM2B-SULF-15	1.08	0.22	36.71	0.09	13.88	48.61	100.60
GOM2B-SULF-23	1.25	0.02	37.61	0.11	12.96	48.39	100.33
GOM2B-SULF-29	1.16	0.03	37.74	0.13	13.16	48.48	100.73
GOM2B-SULF-30	1.13	0.01	37.57	0.11	13.08	48.88	100.78
GOM2B-SULF-35	1.46	0.03	38.62	0.10	11.35	49.99	101.55
GOM2B-SULF-44	1.22	bdl	33.62	0.23	13.50	50.59	99.15
GOM2B-SULF-50	1.16	0.01	37.72	0.12	13.11	47.32	99.46
GOM2B-SULF-70	1.36	bdl	37.41	0.08	13.03	48.69	100.56
$(Ni,Cu)_{11}(Sb,As)_8$							
GOM2B-SULF-40	1.61	0.06	34.62	0.24	6.81	58.53	101.86
breithauptite - NiSb							
GOM2B-SULF-3	2.10	bdl	31.28	0.55	0.02	65.67	99.65
GOM2B-SULF-5	1.97	0.02	31.55	0.09	0.10	65.36	99.09
GOM2B-SULF-6	2.00	0.02	32.13	0.06	0.10	67.05	101.35
GOM2B-SULF-7	1.89	bdl	32.14	0.08	0.06	65.85	100.04
GOM2B-SULF-8	1.76	0.01	32.75	0.03	0.06	65.37	99.98
GOM2B-SULF-14	1.78	bdl	32.10	0.08	0.08	65.77	99.81
GOM2B-SULF-26	1.73	0.02	32.97	0.06	0.07	65.21	100.06
GOM2B-SULF-31	1.79	bdl	34.92	0.08	0.03	64.58	101.41
GOM2B-SULF-34	1.39	0.02	34.12	0.10	0.95	63.56	100.14
GOM2B-SULF-37	1.58	bdl	32.63	0.10	0.18	65.70	100.19
apfu	As	S	Ni	Fe	Cu	Sb	Total
$(Ni,Cu)_{5-x}(Sb,As)_2$							
GOM2B-SULF-1	0.08	0.00	3.66	0.01	1.03	1.99	6.77
GOM2B-SULF-16	0.07	0.00	3.64	0.01	1.03	2.02	6.77
GOM2B-SULF-21	0.07	0.00	3.61	0.01	1.05	2.02	6.77
$(Ni,Cu)_2(Sb,As)$							
GOM2B-SULF-20	0.04	0.00	1.56	0.01	0.47	0.92	3.00
GOM2B-SULF-22	0.04	0.00	1.57	0.00	0.47	0.92	3.00
GOM2B-SULF-15	0.03	0.02	1.48	0.00	0.52	0.95	3.00
GOM2B-SULF-23	0.04	0.00	1.52	0.00	0.49	0.95	3.00
GOM2B-SULF-29	0.04	0.00	1.52	0.01	0.49	0.94	3.00
GOM2B-SULF-30	0.04	0.00	1.52	0.00	0.49	0.95	3.00
GOM2B-SULF-35	0.05	0.00	1.56	0.00	0.42	0.97	3.00
GOM2B-SULF-44	0.04	0.00	1.41	0.01	0.52	1.02	3.00
GOM2B-SULF-50	0.04	0.00	1.54	0.01	0.49	0.93	3.00
GOM2B-SULF-70	0.04	0.00	1.52	0.00	0.49	0.95	3.00
$(Ni,Cu)_{11}(Sb,As)_8$							
GOM2B-SULF-40	0.34	0.03	9.30	0.07	1.69	7.58	19.00
breithauptite - NiSb							
GOM2B-SULF-3	0.05	0.00	0.96	0.02	0.00	0.97	2.00
GOM2B-SULF-5	0.05	0.00	0.97	0.00	0.00	0.97	2.00
GOM2B-SULF-6	0.05	0.00	0.97	0.00	0.00	0.98	2.00
GOM2B-SULF-7	0.05	0.00	0.98	0.00	0.00	0.97	2.00
GOM2B-SULF-8	0.04	0.00	1.00	0.00	0.00	0.96	2.00
GOM2B-SULF-14	0.04	0.00	0.98	0.00	0.00	0.97	2.00
GOM2B-SULF-26	0.04	0.00	1.00	0.00	0.00	0.95	2.00
GOM2B-SULF-31	0.04	0.00	1.03	0.00	0.00	0.92	2.00
GOM2B-SULF-34	0.03	0.00	1.02	0.00	0.03	0.92	2.00
GOM2B-SULF-37	0.04	0.00	0.99	0.00	0.00	0.96	2.00
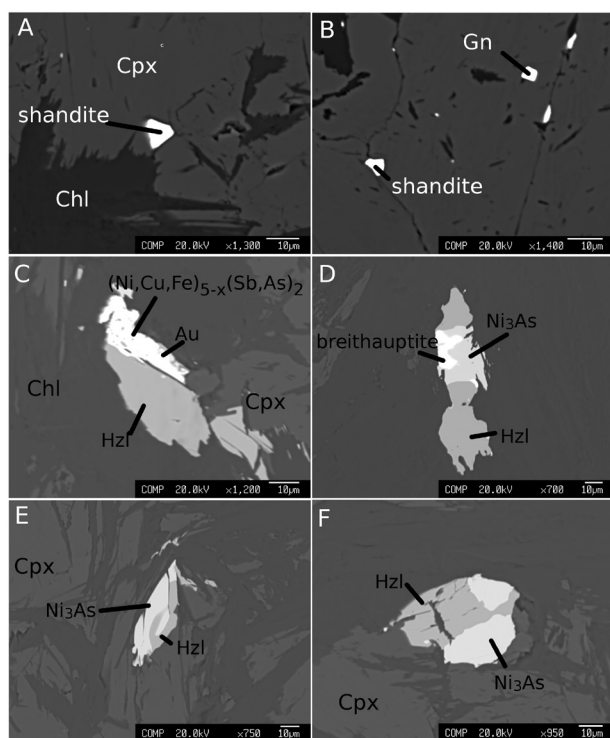
Figure 5. BSE images of Gomati accessory minerals: shandite (A, B), galena (B), heazlewoodite (C, D, E, F), Ni-Cu-Sb-As phases (C, D, E, F). Abbreviations: Cpx=clinopyroxene, Chl=chlorite, Gn=galena, Hzl=heazlewoodite, Au=Au-Cu alloy.
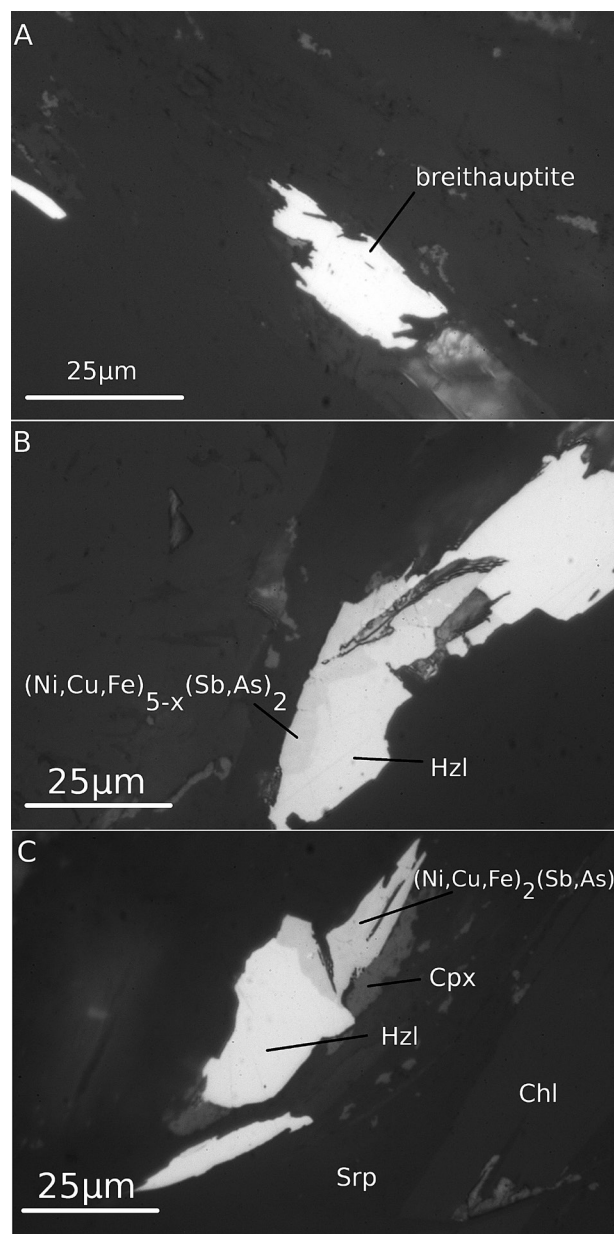

Figure 6. Reflected-light optical images of selected Ni-Cu-Sb-As grains; abbreviations: Srp = serpentine, others like in Figure 5.

properties observed were limited to colour. The optical images of selected Ni-Cu-Sb-As grains are presented in Figure 6 A-C. Under reflected-light breithauptite is yellowish, similar to heazlewoodite (Figure 6A). On the contrary, two Ni-Cu-Fe antimonides show a white-bluish color compared to the associated heazlewoodite found in contact with them (Figure 6 B,C).

DISCUSSION AND CONCLUSIONS
Chemical classification of the Ni-Cu-Sb-As minerals

The electron microprobe analyses show that the Gomati chromitite hosts grains of rare phases in the system Ni-Cu-Sb-As, characterized by a chemistry not previously reported in nature. These observations confirm the results previously presented by Nixon et al. (1990) and Tredoux et al. (2016) that described several minerals in the Ni-Cu-Sb-As system in chromitites from the Alaskan-type Tulameen complex of Canada and from the Bon Accord oxide body, South Africa, respectively. The new compounds analyzed in the Gomati chromitite correspond to the following ideal formulae: Ni_3As, $Ni_5(As,Sb)_2$, $(Ni,Cu)_{5-x}(Sb,As)_2$, $(Ni,Cu)_2(Sb,As)$, $(Ni,Cu)_{11}(Sb,As)_8$ (Figure 4 and Tables 6, 7). According to their compositions and the ternary diagram shown in Figure 4, none of these phases (other

than the breithauptite and orcelite), are listed in the approved minerals by the International Mineralogical Association, as updated in March 2019 (http://cnmnc.main.jp/). The analyses that approach the stoichiometry $(Ni,Cu)_{5-x}(Sb,As)_2$ may correspond to a Sb-analogue of orcelite and the $(Ni,Cu)_{11}(Sb,As)_8$ compound probably represents the Cu-rich Sb-analogue of the mineral maucherite ($Ni_{11}As_8$), also found in the Bon Accord body (Tredoux et al., 2016). The $(Ni,Cu)_2(Sb,As)$ phase has a composition similar to one reported by Nixon et al. (1990)

PM

in the chromitite from Tulameen complex. In case of As-dominant compositions, the following formulae can be suggested: Ni_3As and $Ni_5(As,Sb)_2$. Ni_3As may correspond to the mineral dienerite, formerly discredited by the IMA and only recently under revalidation (Bonazzi and Bindi, 2019). Taking into consideration the small size of some of the analyzed grains and their mode of occurrence, i.e. associated with heazlewoodite, we cannot exclude that a small amount of the detected Ni may be a contribution of the Ni-sulfide. For this reason, some of the calculated stoichiometries may show a slight enrichment in Ni due to the influence of the associated minerals. Although their small size makes very difficult to obtain X-ray diffraction data, we can argue, based on their electron microprobe analyses only, that the following four minerals in the Ni-Cu-Sb-As system have been found in the Gomati chromitite and could represent new mineral species: $Ni_5(As,Sb)_2$, $(Ni,Cu)_{5-x}(Sb,As)_2$, $(Ni,Cu)_2(Sb,As)$, and $(Ni,Cu)_{11}(Sb,As)_8$. Moreover, the Ni_3As detected mineral supports the revalidation of dienerite.

Origin of the accessory minerals in the Gomati chromitite

The experimental studies performed by Raghavan (2004) and Okamoto (2009) on Ni-Fe-Sb alloys (Figure 7), have shown that the phases $NiSb$, Ni_3Sb and Ni_7Sb_3 are stable over a wide temperature range, but Ni_5Sb_2 only occurs at temperatures in excess of 600 °C. This last phase has not been observed in the Gomati chromitite, thus implying that the crystallization of the antimonides in the studied sample may have occurred at temperatures lower than 600 °C, or even less if we consider that the presence of impurities within the antimonides in Gomati could have further lowered the temperature. This assumption is also supported by the presence of other accessory minerals such as heazlewoodite and shandite that are believed to crystallize during serpentinization of ultramafic rocks. Their maximum thermal stability is 556 °C for heazlewoodite (Tzamos et al., 2016) and about 500 °C for shandite (Zhmodik and Agafonov, 2000). The origin at low temperature of the minerals in the Ni-Cu-Sb-As system as well as the associated accessory minerals found in the Gomati chromitite is consistent also with the temperature registered by the analysed chlorite that is comprised between 220 and 310 °C.

The source of the metals in the Ni-As-Cu-Sb system is currently unknown. Minerals in the Ni-As-Sb-Ag-Au-Cu have also been found within other ultramafic complexes, like the Ognit Complex (Shvedov and Barkov, 2017; Barkov et al., 2019), where Authors suggest that the formation of these phases may be related to cooling in a fluid-enriched system.

Ultramafic rocks contain nickel and arsenic that may have a magmatic origin or can be related with the alteration
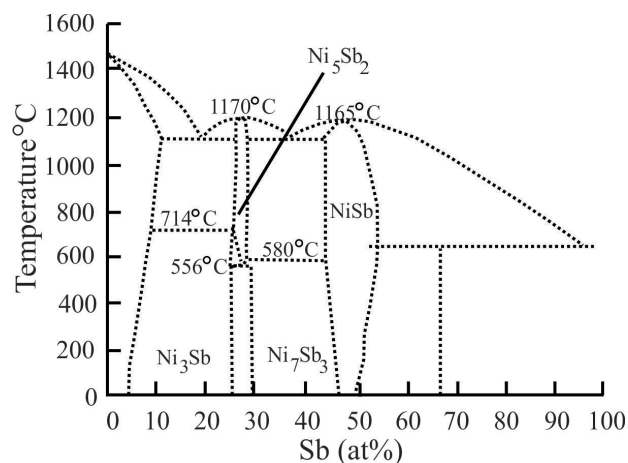

Figure 7. Temperature stability and phase relations in the Fe-Ni-Sb system, as proposed by Okamoto (2009).

of their host rocks during serpentinization (Prichard et al., 2008; Kapsiotis et al., 2011). However, the presence in Gomati of abundant minerals containing Sb, such as breithauptite, $(Ni,Cu)_{5-x}(Sb,As)_2$, $(Ni,Cu)_2(Sb,As)$, and $(Ni,Cu)_{11}(Sb,As)_8$, together with tetraauricupride, galena and chalcocite, described in the present work, as well as native silver (Economou, 1984), supports the hypothesis that Sb, Pb, Cu, Au and Ag were metasomatically added during cooling. These hydrothermal fluids could have been emanated from the granite occurring in contact with the Gomati ophiolite (Figure 1). A similar mechanism was proposed for the crystallization of exotic minerals described in the Campo Formoso layered chromitites of Brazil (Zaccarini et al., 2006). Another possible source is the Sb-rich porphyry mineralisation occurring in the area (Tzamos et al., 2019), which could have contributed to the addition of these metals through migrating fluids transported within fault zones.

The occurrence of a metasomatic event in the Gomati chromitite was reported also by Scarpelis and Economou (1978), thus confirming the activity of a fluid phase in the Gomati chromite forming system, that can be considered the responsible for the crystallization of the rare and accessory phases described in this contribution.

REFERENCES

Barkov A.Y., Bindi L., Tamura N., Shvedov G.I., Winkler B., Stan C.V., Morgenroth W., Martin F., Zaccarini F., Stanley

C.J., 2019. Ognitite, NiBiTe, a new mineral species, and cobaltian maucherite from the Ognit ultramafic complex, Eastern Sayans, Russia. Mineralogical Magazine, 1-25.

Bayliss P., 1990. Revised unit-cell dimensions, space group, and chemical formula of some metallic minerals. The Canadian Mineralogist 28, 751-755.

Bayliss P., 1991. Crystal chemistry and crystallography of some minerals in the tetradymite group. American Mineralogist 76, 257-265.

Bindi L., Tredoux M., Zaccarini F., Miller D.E., Garuti G., 2014. Non-stoichiometric nickel arsenides in nature: the structure of orcelite, $Ni_{5-x}As_2$ (x=0.25), from the Bon Accord oxide body, South Africa. Journal of Alloys and Compounds 601, 175-178.

Bonev N., Dilek Y., Hanchar J.M., Bogdanov K., Klain L., 2012. Nd-Sr-Pb isotopic composition and mantle sources of Triassic rift units in the Serbo-Macedonian and the western Rhodope massifs (Bulgaria-Greece). Geological Magazine 149, 146-152.

Bonev N., Moritz R., Borisova M., Filipov P., 2018. Therma-Volvi-Gomati complex of the Serbo-Macedonian Massif, northern Greece: a Middle Triassic continental margin ophiolite of Neotethyan origin. Journal of the Geological Society of London 176.5, 931-944.

Cabri L.J., Harris D.C., Stewart J.M., 1970. Paracostibite (CoSbS) and nisbite ($NiSB_2$), new minerals from the Red Lake area, Ontario, Canada. The Canadian Mineralogist 10, 232-246.

Cathelineau M., 1988. Cation site occupancy in chlorites and illites as a function of temperature. Clay Minerals 23, 471-485.

Cathelineau M. and Nieva D., 1985. A chlorite solid solution geothermometer the Los Azufres (Mexico) geothermal system. Contributions to Mineralalogy and Petrology 91, 235-244.

Christodoulou C., 1980. The Geochemistry of podiform chromite deposits from two ophiolite complexes, Chalkidiki peninsula, Northern Greece. Dissertation Durham University.

Dixon J.E. and Dimitriadis S., 1984. Metamorphosed ophiolitic rocks from the Serbo-Macedonian Massif, near Lake Volvi, north-east Greece. Geological Society, London, Special Publications 17, 603-618.

Economou M., 1984. On the chemical composition of the chromite ores from the Chalkidiki peninsula, Greece. Ofioliti 123-134.

Frimmel H.E., 1997. Chlorite thermometry in the Witwatersrand Basin: constraints on the Paleoproterozoic geotherm in the Kaapvaal Craton, South Africa. The Journal of Geology 105, 601-616.

Hey M.H., 1954. A new review of the chlorites. Mineralogical Magazine and Journal of the Mineralogical Society 30, 277-292.

Iglesias J.E. and Nowacki W., 1977. Refinement of the crystal structure of α domeykite, a structure related to the A15 type.

Zeitschrift für Kristallographie-Crystalline Materials 145, 334-345.

Johan Z., 1961. Paxite-Cu_2As a New Copper Arsenide Černỳ Důl in the Giant Mts.(Krkonoše). Acta Universitatis Carolinae, Geologica 2, 77-86.

Johan Z., 1958. Koutekite: a new mineral. Nature 181, 1553-1554.

Johan Z. and Hak J., 1961. Novákite,$(Cu,Ag)_4As_3$, a new mineral. American Mineralogist: Journal of Earth and Planetary Materials 46, 885-891.

Kabalov Y.K., Sokolova E.V., Spiridonov E.M., Spiridonov F.M., 1994. Crystal structure of a new mineral $CuNiSb_2$. Physics-Doklady 335, 709-711.

Kapsiotis A., Grammatikopoulos T.A., Tsikouras B., Hatzipanagiotou K., Zaccarini F., Garuti G., 2011. Mineralogy, composition and PGM of chromitites from Pefki, Pindos ophiolite complex (NW Greece): evidence for progressively elevated fAs conditions in the upper mantle sequence. Mineralogy and Petrology 101, 129-150.

Kockel F., 1977. Erläuterungen zur Geologischen Karte der Chalkidhiki und angrenzender Gebiete 1:100000 (Nord-Griechenland). Bundesanstalt für Geowissenschaften und Rohstoffe.

Kranidiotis P. and MacLean W.H., 1987. Systematics of chlorite alteration at the Phelps Dodge massive sulfide deposit, Matagami, Quebec. Economic Geology 82, 1898-1911.

Leonard B.F., Mead C.W., Finney J.J., 1971. Paradocrasite, $Sb_2(Sb,As)_2$, a new mineral. American Mineralogist: Journal of Earth and Planetary Materials 56, 1127-1146.

Liebisch W. and Schubert K., 1971. Zur struktur der Mischung Kupfer-Arsen. Journal of the Less Common Metals 23, 231-236.

Makovicky E. and Merlino S., 2009. OD (order-disorder) character of the crystal structure of maucherite Ni_8As_{11}. European Journal of Mineralogy 21, 855-862.

Melfos V. and Voudouris P.C., 2012. Geological, Mineralogical and Geochemical Aspects for Critical and Rare Metals in Greece. Minerals 2, 300-317.

Morimoto N., Fabries J., Ferguson A.K., Ginzburg I.V., Ross M., Seifert F.A., Zussman J., 1988. Nomenclature of pyroxenes. Mineralogical Magazine 52, 535-550.

Nixon G.T., Cabri L.J., Laflamme J.H.G., 1990. Platinum-group-element mineralization in lode and placer deposits associated with the Tulameen Alaskan-type complex, British Columbia. The Canadian Mineralogist 28, 503-535.

Okamoto H., 2009. Ni-Sb (Nickel-Antimony). Journal of Phase Equilibria and Diffusion 30, 301-302.

Palache C., Berman H., Frondel C., 1944. The System of Mineralogy, vol. I - elements, sulfides, sulfosalts and oxides. New York 238-239.

Peacock M.A., 1939. Rammelsbergite and parammelsbergite, distinct orthorhombic forms of $NiAs_2$. American Mineralogist: Journal of Earth and Planetary Materials 24, 10-11.

Peacock M.A. and Dadson A.S., 1940. On rammelsbergite and pararammelsbergite: distinct forms of nickel diarsenide. American Mineralogist: Journal of Earth and Planetary Materials 25, 561-577.

Pearson W.B., 1985. The Cu_2Sb and related structures. Zeitschrift für Kristallographie-Crystalline Materials 171, 23-39.

Prichard H.M., Economou-Eliopoulos M., Fisher P.C., 2008. Platinum-group minerals in podiform chromitite in the Pindos ophiolite complex, Greece. Canadian Mineralogist 46, 329-341.

Raghavan V., 2004. Fe-Ni-Sb (Iron-Nickel-Antimony). Journal of Phase Equilibria and Diffusion 25, 553.

Ricou L., Burg J., Godfriaux I., Ivanov Z., 1998. Rhodope and Vardar : the metamorphic and the olistostromic paired belts related to the Cretaceous subduction under Europe. Geodinamica Acta 11, 285-309.

Scarpelis N. and Economou M., 1978. Genesis and metasomatism of chromite ore from the Gomati area, Chalkidiki, Greece. Ann. Geol. Pays Hell 29, 716-728.

Schumer B.N., Andrade M.B., Evans S.H., Downs R., 2017. A new formula and crystal structure for nickelskutterudite, $(Ni,Co,Fe)As_3$, and occupancy of the icosahedral cation site in the skutterudite group. American Mineralogist 102, 205-209.

Şengör A.M.C., Yılmaz Y., Sungurlu O., 1984. Tectonics of the Mediterranean Cimmerides: nature and evolution of the western termination of Palaeo-Tethys. Geological Society, London, Special Publications 17, 77-112.

Shvedov G.I. and Barkov A.Y., 2017. Primary and alteration assemblages of platinum-group minerals from the Ognit complex, Irkutskaya oblast, Eastern Sayans, Russia. Neues Jahrbuch für Mineralogie-Abhandlungen: Journal of Mineralogy and Geochemistry, 194, 35-48.

Thompson J.G., Rae A.D., Withers R.L., Welberry T.R., Willis A.C., 1988. The crystal structure of nickel arsenide. Journal of Physics C: Solid State Physics 22, 4007-4016.

Tredoux M., Roelofse F., Shukolyukov A., 2014. A Cr isotopic study of the Bon Accord NiO body in the Barberton greenstone belt, South Africa. Chemical geology 390, 182-190.

Tredoux M., Zaccarini F., Garuti G., Miller D.E., 2016. Phases in the Ni-Sb-As system which occur in the Bon Accord oxide body, Barberton greenstone belt, South Africa. Mineralogical Magazine 80, 187-198.

Tzamos E., Filippidis A., Michailidis K., Koroneos A., Rassios A., Grieco G., Pedrotti M., Stamoulis K., 2016. Mineral chemistry and formation of awaruite and heazlewoodite in the Xerolivado chrome mine, Vourinos, Greece. Bulletin of the Geological Society of Greece 50, 2047-2056.

Tzamos E., Papadopoulos A., Grieco G., Stoulos S., Bussolesi M., Daftsis E., Vagli E., Dimitriadis D., Godelitsas A., 2019. Investigation of Trace and Critical Elements (Including Actinides) in Flotation Sulphide Concentrates of Kassandra Mines (Chalkidiki, Greece). Geosciences, 9, 164.

Vinogradova R.A., Rudashevskii N.S., Bud'ko I.A., Bochek L.I.,

Kaspar P., Padera K., 1977. Krutovite - a new cubic nickel diarsenide. International Geology Review, 19, 232-244.

Zaccarini F., Garuti G., Martin R.F., 2006. Exotic accessory minerals in layered chromitites of the Campo Formoso complex Brazil). Geologica Acta: an international earth science journal 4, 461-469.

Zang W. and Fyfe W.S., 1995. Chloritization of the hydrothermally altered bedrock at the Igarapé Bahia gold deposit, Carajás, Brazil. Mineralium Deposita 30, 30-38.

Zhmodik S.M. and Agafonov L.V., 2000. Shandite and other nickel minerals from chromitites of ophiolite association in the southeast of East Sayan. Geologiya i Geofizika 41, 712-721.